JOURNAL OF NANO- AND ELECTRONIC PHYSICS
Vol. **17** No 2, 02006(11pp) (2025)

ЖУРНАЛ НАНО- ТА ЕЛЕКТРОННОЇ ФІЗИКИ
Том **17** № 2, 02006(11cc) (2025)

OPEN ACCESS

REGULAR ARTICLE

The Effect of Geometry on Thermoplasmonic Phenomena in Metallic Nanoparticles

V.I. Reva[1], R.Yu. Korolkov[1], M.A. Shvydkyi[1], A.V. Korotun[1,2,*], E.V. Stegantsev[3], O.S. Hnatenko[1,4]

[1] *National University Zaporizhzhia Polytechnic, 69063 Zaporizhzhia, Ukraine*
[2] *G.V. Kurdyumov Institute for Metal Physics, N.A.S. of Ukraine, 03142 Kyiv, Ukraine*
[3] *Zaporizhzhia National University, 69600 Zaporizhzhia, Ukraine*
[4] *Kharkiv National University of Radio Electronics, 61166 Kharkiv, Ukraine*

(Received 16 February 2025; revised manuscript received 24 April 2025; published online 28 April 2025)

The work investigates thermoplasmonic phenomena in metallic nanoparticles of the different geometry. The relations for the frequency dependences of nanoparticle overheating and radiation efficiency, as well as the size dependence of Joule number, which characterizes the ability of nanoparticles to generate heat, were obtained. At the same time, the size dependences of the effective electron relaxation rate for cylindrical and disk particles are determined within the frameworks of the equivalent spheroid approach. The frequency dependences of polarizability, absorption and scattering cross-sections, overheating, radiation efficiency and the size dependences of Joule number were calculated for spherical, cylindrical and disk nanoparticles of the different sizes and different metals. It is shown that the number and positions of maxima of absorption and scattering cross-sections and overheating of metallic nanoparticles depend on their geometry and, in the case of 1*D*-particles, on their sizes (aspect ratio). The splitting of these maxima for cylindrical particles is significantly greater than for disk particles. The calculations demonstrate that the overheating of nanoparticles in the biological transparency windows ranges from fractions to a few degrees, except in the case of nanocylinders with the small aspect ratio, where the overheating maxima of silver nanoparticles fall within the first biological transparency window. It was established that the material of nanoparticles also significantly affects the position of their overheating maximum and is determined by the value of the plasma frequency. It is demonstrated the feasibility of using spherical, disk and short cylindrical nanoparticles in applications where negligible overheating in biological transparency windows is required. In the cases where the significant overheating is required, the use of long nanocylinders is appropriate. Fundamental differences in the behavior of Joule number (ability to generate heat) for particles of different geometries under the variation of their radius / aspect ratio have been found.

Keywords: Polarizability, Absorption cross-section and scattering cross-section, Overheating, Radiation efficiency, Joule number, Effective relaxation rate.

DOI: 10.21272/jnep.17(2).02006 PACS numbers: 73.20.Mf, 78.20.Nv, 78.67.Bf

1. INTRODUCTION

Thermonanoplasmonics is becoming one of the main directions of plasmonics and is the combination of nanooptics and nanothermodynamics. The heat generation in plasmonic nanoparticles due to the absorption of electromagnetic wave, has long been considered as a parasitic effect, the influence of which had to be reduced. Recently, however, it has been found that nanoparticles can be converted into efficient nanoscale heat sources [1, 2]. In this case, the plasmonic nanoparticles as heat sources are remotely controlled by the laser, which opens up prospects for controlling the temperature distribution at the nanoscale [3]. The most popular plasmonic nanoparticles are gold, silver, and copper particles, which have significant free electron density of the order of $10^{20}-10^{23}$ cm^{-3} and resonant frequency, which is in the visible or near-infrared region of the spectrum [4, 5].

The ability of metallic nanoparticles to scatter and absorb light depends on the nature of the metal, the geometry of the particle, the properties of the environment and the electromagnetic wavelength (frequency). The geometry and size of metallic nanoparticle can itself significantly alter its ability to scatter and absorb light [6-8]. For example, when Au, Ag, or Cu metal nanoparticles are rod-shaped, the longitudinal surface plasmonic resonance (SPR) shifts from the visible to the near-infrared frequency range [9].

In recent years, the use of metallic nanostructures for heat delivery in many photothermal applications has been the subject of numerous research, ranging from solar energy harvesting, where plasmonic nanostructures have been used to improve the efficiency of solar energy absorption [10-13], to biomedical research, where tissue temperature control has been widely used for therapeutic purposes in several medical fields such as oncology, physiotherapy, urology, cardiology and ophthalmology [14, 15]. Photothermal therapy (PTT), for example, is the technique based on the induction of cellular damage by absorbing light in the target tissue [16-18]. High-performance PTT is

* Correspondence e-mail: andko@zp.edu.ua

Cite this article as: V.I. Reva et al., *J. Nano- Electron. Phys.* 17 No 2, 02006 (2025) https://doi.org/10.21272/jnep.17(2).02006

achieved when metallic nanoparticles are used as nanoheaters for localized photothermal conversion. Among the applications that utilize one or more nanoparticles, laser-mediated generation of microbubbles stands out [19, 20]. The generation of microbubbles using metallic nanoparticles leads to photoporation of the cell membrane for intracellular delivery of molecules [21-23]. In addition, ultrafast photothermal processes in the neighborhood of nanoparticles have also been proposed as an alternative method for optical switching in communication devices [24].

The use of infrared (IR) light sources for biomedical applications in the biological window of transparency allows deep tissue treatment (in the range of several centimeters) due to negligible absorption and scattering. Two spectral bands are ideal for the optical therapy of deep tissues [25]:

1) the first biological transparency window – occupies the range from 700 nm to 980 nm;

2) the second biological transparency window – occupies the range from 1000 nm to 1400 nm.

Various methods exist for preparing nanoparticles, which have the large cross-section and tunable plasmonic spectrum in the IR range. The great values of the absorption cross-section in IR range can be achieved by nanoparticles of the different shapes such as rods [26], shells [27, 28] and cages [16, 29]. In particular, metallic nanorods possess exceptional tunability of the spectral positions of the longitudinal and transverse surface plasmonic resonances [30], which makes them an attractive candidate for biomedical applications. However, infrared optical therapy raises concerns about its availability from the clinical stand point. For example, laser exposure of human skin at 1064 nm is limited in power to 100 mJ/cm^2 for laser pulses of less than 100 ns duration and 1 W/cm^2 for continuous illumination [31]. Therefore, in photothermal therapy using plasmonic particles, the use of high-performance metallic nanoparticle heaters may lead to both a decrease in the concentration of nanoparticles used and a decrease in the luminous flux.

Let us note that in [32, 33] the maximum overheating of bimetallic nanoparticles of the different composition was evaluated, and in [34] – spherical metallic nanoparticles coated with the layer of J-aggregate was evaluated. In [35] frequency dependences of the overheating of spherical bimetallic nanoparticles are analyzed, and in [36] temperature distributions in biological tissues in the neighborhood of spherical nanoparticles of the different structure and composition are studied. However, the issue of determining the possibilities of practical use of the overheating of nanoparticles of non-spherical geometry is practically unexplored, which determines its relevance.

2. MODEL OF THERMAL PHENOMENA IN PLASMONIC NANOPARTICLES

2.1 Thermal Phenomena in Metallic Nanoparticles, Induced by Surface Plasmons

When radiation hits metallic nanostructure, exciting surface plasmonic resonances, the absorbed light energy promotes the transition of electrons to an excited state above Fermi level of metal, changing the population distribution of the conduction band as shown in Figure 1, *a*. In this case, electron-electron scattering will contribute to the thermalization of charge carriers (Fig. 1, *b*). The interaction time of hot electrons with the nanocrystal lattice is $\sim 10^{-12}$ s, which corresponds to the intrinsic characteristic relaxation time of electrons and phonons. As shown in Fig. 1, *c*, the thermal energy is then released to the surrounding environment, mainly by heat transfer, causing the nanoparticle to act as the nanoheater. The characteristic thermal relaxation time of metallic nanoparticle depends on its size and is described by the relation [37]:

$$\tau_d = \frac{\rho c_p}{3\kappa} R_{\text{eq}}^2 , \qquad (1)$$

where R_{eq} is the equivalent radius of sphere, the volume of which is equal to the volume of metallic nanoparticle of any shape; ρ and c_p are the density and specific heat capacity of metal correspondingly, and κ is thermal conductivity of the environment. In water τ_d for metallic nanoparticle can reach few nanoseconds.

When incident light hits the plasmonic nanoparticle, it is scattered and absorbed, thereby causing energy loss of the incident light. From a quantitative point of view, all three processes can be characterized by the absorption, scattering and extinction cross-sections C_{abs}, C_{sca} and C_{ext}, which are the ratio of the respective powers $W_{\text{abs, sca, ext}}$ to the incident light intensity I_0 [38]. Consequently, the integral cross-sections have the dimension of area and are proportional to the corresponding energies. An equality $C_{\text{ext}} = C_{\text{abs}} + C_{\text{sca}}$ follows from the law of conservation of energy. The electric field displaces free electrons from metal and creates uncompensated charges near the particle surface and restoring forces. Due to the collective behavior, the resonant frequency of such an oscillator does not coincide with the frequency of light ω.

When choosing the shape of metallic nanoparticles for thermal applications, structures with large absorption cross-section C_{abs} are desirable. Greater values C_{abs} lead to the significant absorption of light energy and, hence, the increase in the nanoparticle temperature. In general, when the size of the plasmonic particles increases, not only the absorption cross-section increases, but also the value of the scattering cross-section C_{sca} increases. However, for bigger particles, the scattering process begins to determine the interaction of light with nanoparticles. In this case, the light energy is strongly scattered by the nanoparticles into the surrounding environment. Thus, photothermal conversion efficiency (radiation efficiency) ξ_{rad} is known as an important index in evaluating the relationship between optical characteristics and nanoparticle heating [39, 40], which is defined by the relation

$$\xi_{\text{rad}} = \frac{1}{1 + \dfrac{C_{\text{sca}}}{C_{\text{abs}}}} , \qquad (2)$$

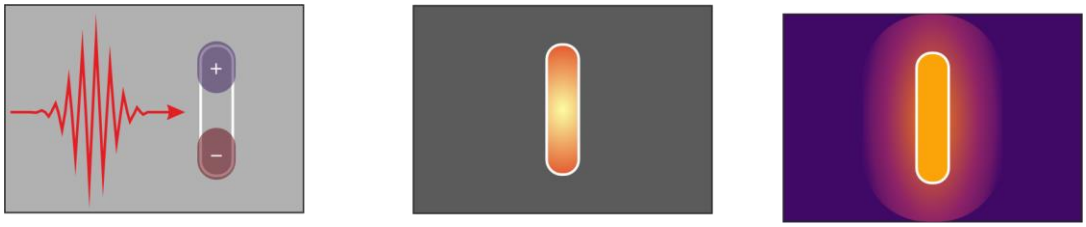

a b c

Fig. 1 – The illustration of the dynamics of photothermal phenomena in the neighborhood of metallic nanoparticles: *a* – transition of electrons to the conduction zone under the action light (fs); *b* – electron-phonon relaxation (ps), *c* – heat exchange with the environment (ps to ns)

The value ξ_{rad} quantifies the fraction of the incident electromagnetic wave energy absorbed by the nanostructure. The ability of nanoparticles to radiate heat into the surrounding medium is associated with their surface area and volume. In order to allow the greater heat loss, volume must be minimized and the surface area must be maximized. Thus, the morphology of nanoparticles becomes relevant for thermoplasmonics applications. Thus, [41] describes an effective way to estimate the ability of nanoparticles to generate heat using the Joule number Jo , which is defined as

$$J_0 = \frac{c}{\omega_{\text{ref}}} \frac{C_{\text{abs}}}{V}, \tag{3}$$

where ω_{ref} is the reference frequency of photon with the given energy. Alternatively, [42] investigated the Arrhenius integral describing irreversible thermal damage as the function of the size of gold nanoparticles in order to estimate the efficiency of localized hyperthermia and showed that the absorption efficiency of nanoparticles may be insufficient for the determination of photothermal damage to biological tissues. In addition, [43] showed that the absorption of Au nanoparticles and the temperature rise during photothermal heating strongly depend on the shape and size of the nanoparticles.

The plasmonic heating induced by pulsed lasers and continuous radiation sources is controlled by different dynamics and therefore depends on the laser characteristics, which should also be taken into account for the selection of the efficient nanoheaters.

Light absorption is the key process for PTT applications because of the time-efficient and nanoscale conversion of electromagnetic energy into the thermal energy. Briefly, the physics underlying this process can be described as follows (Figure 2) [44]. The absorbed laser pulse rapidly creates, on the timescale of less than 100 fs, the non-thermal distribution of the energy of electrons. The thermal distribution of electrons with the characteristic time of less than one picosecond is established due to electron-electron scattering. Due to the low heat capacity of conduction electrons, huge electron temperatures ($\sim 1000-5000$ K) can be easily achieved in nanoparticles even at low pulse energies of ~ 100 nJ. Thermalized hot electrons cause lattice heating due to electron-phonon (e-ph) processes within 1-5 ps. As a rule, the particle temperature is tens of degrees higher than the initial temperature. The heating of the lattice is accompanied by its cooling due to the dissipation of heat from the particle into the environment. Since the nanoparticle size is less than 100 nm, the heating of the medium is highly localized near the particle on the nanometre scale. This property is crucial for targeted and localized PTT without damaging healthy cells and tissues.

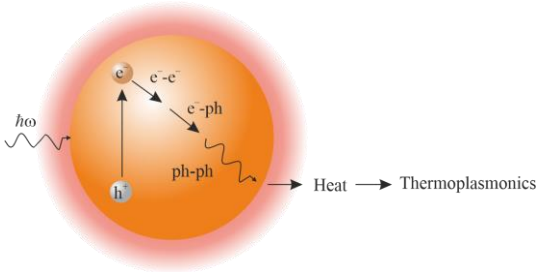

Fig. 2 – To the explanation of the thermal phenomena in the neighborhood of nanoparticle

The following two optical parameters of plasmonic nanoparticles should be adequately tuned for in vivo PTT applications: (1) the wavelength (frequency) of the plasmonic resonance and (2) the scattering/absorption $C_{\text{sca}}/C_{\text{abs}}$ or absorption/extinction $C_{\text{abs}}/C_{\text{ext}}$ ratio. In order to avoid unwanted absorption of light by water and hemoglobin and scattering by inhomogeneous tissue structures, radiation from the near infrared or shortwave and visible infrared part of the spectrum should be used. In order to maximize the efficiency of light-to-heat conversion, nanoparticles with the minimum ratio of $C_{\text{sca}}/C_{\text{abs}}$ should be used.

2.2 Statement of the Problem

Let us assume that the spherical metallic nanoparticle with the radius R is in medium with the dielectric permittivity ϵ_{m}. When excitation of surface plasmonic resonances occurs, the overheat of nanoparticle takes place, the value of which is determined by the solution of the system of one-dimensional stationary heat conduction equations

$$\begin{cases} \frac{1}{r^2}\frac{d}{dr}\left(r^2\kappa_0\frac{dT_1}{dr}\right) = -q; \\ \frac{1}{r^2}\frac{d}{dr}\left(r^2\kappa\frac{dT_2}{dr}\right) = 0 \end{cases} \tag{4}$$

with the cross-linking boundary conditions at the boundary between the nanoparticle and the environment

$$\begin{cases} T_1(R) = T_2(R); \\ \kappa_0 \left.\dfrac{dT_1}{dr}\right|_{r=R} = \kappa \left.\dfrac{dT_2}{dr}\right|_{r=R}, \end{cases} \tag{5}$$

where T_1 and T_2 are temperatures of particle and environment; q is external heat flux density; κ_0 is heat conductivity coefficient of nanoparticle material.

The solution of the formulated problem (4) – (5) has the form

$$\begin{cases} T_1(r) = \dfrac{q}{4\pi\kappa R}\left(1 + \dfrac{\kappa}{\kappa_0}\left(1 - \dfrac{r^2}{R^2}\right)\right) + T_\infty; \\ T_2(r) = \dfrac{q}{4\pi\kappa r} + T_\infty. \end{cases} \tag{6}$$

Since in practice $\kappa/\kappa_0 \ll 1$, then formulae (6) take the form

$$\begin{cases} T_1(r) = \dfrac{q}{4\pi\kappa R} + T_\infty; \\ T_2(r) = \dfrac{q}{4\pi\kappa r} + T_\infty. \end{cases} \tag{7}$$

The overheating of spherical nanoparticle under light irradiation

$$\Delta T = T_1 - T_\infty = \frac{q}{4\pi\kappa R}, \tag{8}$$

and since the heat flux density

$$q = C_{\text{abs}} I_0, \tag{9}$$

where I_0 is the intensity of radiation incident on the nanoparticle, then from (8) and (9) we obtain the expression

$$\Delta T = \frac{C_{\text{abs}} I_0}{4\pi\kappa R}, \tag{10}$$

If one introduces β and R_{eq} are the shape parameter and equivalent radius of the nanoparticle, then formula

$$\Delta T = \frac{C_{\text{abs}} I_0}{4\pi\kappa\beta R_{\text{eq}}} \tag{11}$$

can be applied for the nanoparticles of cylindrical and disc shape.

It is clear that for the spherical nanoparticle

$$\beta = 1, \; R_{\text{eq}} = R, \tag{12}$$

while for nanocylinder and nanodisc the equivalent radius can be obtained from the condition of the equality of the volumes of full sphere and cylinder / disk

$$V_{\text{sph}} = V_{\text{cyl}}, \qquad V_{\text{sph}} = V_{\text{disk}}, \tag{13}$$

where

$$V_{\text{sph}} = \frac{4}{3}\pi R^3, \qquad V_{\text{cyl}} = \frac{\pi}{4} d^2 l, \qquad V_{\text{disk}} = \frac{\pi}{4} d^2 h,$$

l is the length of cylinder; h is the height of disc; d is the diameter of cylinder / disc.

Thus the expressions for the equivalent radiuses of cylinder / disc have the form, correspondingly:

$$R_{\text{eq}}^{\text{cyl}} = \frac{1}{2}\sqrt[3]{\frac{3}{2} d^2 l}, \; R_{\text{eq}}^{\text{disk}} = \frac{1}{2}\sqrt[3]{\frac{3}{2} d^2 h}, \tag{14}$$

In turn, the relations for cylinder / disc shape parameter:

$$\beta_{\text{cyl}} = 1 + 0.96587 \ln^2\left(\frac{l}{d}\right), \tag{15}$$

$$\begin{aligned} \beta_{\text{disk}} = \exp\Bigg\{ & 0{,}040 - 0{,}0124 \ln\left(\frac{h}{d}\right) + \\ & + 0{,}0677 \ln^2\left(\frac{h}{d}\right) - 0{,}00457 \ln^3\left(\frac{h}{d}\right)\Bigg\}. \end{aligned} \tag{16}$$

The absorption and scattering cross-sections for nanoparticles of the considered shapes are determined by the expressions

$$\begin{aligned} C_{\text{abs}} &= \frac{\omega}{c}\sqrt{\epsilon_{\text{m}}}\left(\frac{2}{3}\operatorname{Im}\alpha_\perp + \frac{1}{3}\operatorname{Im}\alpha_\parallel\right), \\ C_{\text{sca}} &= \frac{1}{6\pi}\frac{\omega^4}{c^4}\epsilon_{\text{m}}^2\left(\frac{2}{3}|\alpha_\perp|^2 + \frac{1}{3}|\alpha_\parallel|^2\right), \end{aligned} \tag{17}$$

where the diagonal components of the polarizability tensor

$$\alpha_{\perp(\parallel)}(\omega) = V \frac{\epsilon_{\perp(\parallel)}(\omega) - \epsilon_{\text{m}}}{\epsilon_{\text{m}} + \mathcal{L}_{\perp(\parallel)}\left(\epsilon_{\perp(\parallel)}(\omega) - \epsilon_{\text{m}}\right)}, \tag{18}$$

and the diagonal components of the dielectric tensor of nanoparticle material have the following form within Drude model:

$$\epsilon_{\perp(\parallel)}(\omega) = \epsilon^\infty - \frac{\omega_p^2}{\omega\left(\omega + \mathrm{i}\,\gamma_{\text{eff}}^{\perp(\parallel)}\right)}. \tag{19}$$

In formulas (18) and (19): V is the volume of nanoparticle; $\mathcal{L}_{\perp(\parallel)}$ are depolarization factors; ϵ^∞ is the contribution of the interzone transitions into the dielectric function; ω_p is plasma frequency, and the effective relaxation rate

$$\gamma_{\text{eff}}^{\perp(\parallel)} = \gamma_{\text{bulk}} + \gamma_{\text{s}}^{\perp(\parallel)} + \gamma_{\text{rad}}^{\perp(\parallel)}, \tag{20}$$

where the bulk relaxation rate $\gamma_{\text{bulk}} = \text{const}$ for each metal; $\gamma_{\text{s}}^{\perp(\parallel)}$ and $\gamma_{\text{rad}}^{\perp(\parallel)}$ are surface relaxation rate and radiation damping rate.

2.3 Overheating of Spherical, Cylindrical and Disk Nanoparticles

We now concretize the above theory for spherical, cylindrical and disc nanoparticles.

For the spherical particles $\mathcal{L}_\perp = \mathcal{L}_\parallel = 1/3$, hence, the relations (17) – (20) take the form

$$C_{\text{abs}} = \frac{\omega}{c}\sqrt{\epsilon_{\text{m}}}\,\text{Im}\,\alpha, \qquad C_{\text{sca}} = \frac{1}{6\pi}\frac{\omega^4}{c^4}\epsilon_{\text{m}}^2\left|\alpha\right|^2; \tag{21}$$

$$\alpha_\perp = \alpha_\parallel = \alpha(\omega) = 3V\frac{\epsilon(\omega)-\epsilon_{\text{m}}}{\epsilon(\omega)+2\epsilon_{\text{m}}}; \tag{22}$$

$$\epsilon_\perp = \epsilon_\parallel = \epsilon(\omega) = \epsilon^\infty - \frac{\omega_p^2}{\omega(\omega+\text{i}\,\gamma_{\text{eff}})}; \tag{23}$$

$$\gamma_{\text{eff}} = \gamma_{\text{bulk}} + \gamma_{\text{s}} + \gamma_{\text{rad}}, \tag{24}$$

where

$$\gamma_{\text{s}} = \mathcal{A}(\omega, R)\frac{v_{\text{F}}}{R}; \tag{25}$$

$$\gamma_{\text{rad}} = \frac{V}{6\pi}\sqrt{\frac{\epsilon^\infty+2\epsilon_{\text{m}}}{\epsilon_{\text{m}}}}\left(\frac{\omega_p}{c}\right)^3\mathcal{A}(\omega, R)\frac{v_{\text{F}}}{R}, \tag{26}$$

and the effective parameter describing the degree of coherence loss at electron scattering on the surface

$$\mathcal{A}(\omega, R) = \frac{3}{4}\frac{1}{\epsilon^\infty+2\epsilon_{\text{m}}}\left(\frac{\omega_p}{\omega}\right)^2 \times \times\left[1-\frac{2v_s}{\omega}\sin\frac{\omega}{v_s}+\frac{2v_s^2}{\omega^2}\left(1-\cos\frac{\omega}{v_s}\right)\right], \tag{27}$$

$v_s = v_{\text{F}}/2R$ is the frequency of the individual oscillations of electrons; v_{F} is Fermi electron velocity.

For cylindrical and disc nanoparticles, the equivalent of which are prolate and oblate spheroids, respectively, expressions (17) – (20) retain their form, and the surface relaxation rate and radiation damping rate are given by the expressions:

$$\gamma_{\text{s}}^{\perp(\parallel)} = \frac{9}{16}\frac{\mathcal{L}_{\perp(\parallel)}}{\epsilon_{\text{m}}+\mathcal{L}_{\perp(\parallel)}(1-\epsilon_{\text{m}})}\left(\frac{\omega_p}{\omega}\right)^2\frac{v_{\text{F}}}{2R}\mathcal{F}_{\perp(\parallel)}(\varrho_{\text{eff}}); \tag{28}$$

$$\gamma_{\text{rad}}^{\perp(\parallel)} = \frac{V}{8\pi}\frac{\mathcal{L}_{\perp(\parallel)}}{\sqrt{\epsilon_{\text{m}}\left[\epsilon^\infty+\left(\frac{1}{\mathcal{L}_{\perp(\parallel)}}-1\right)\epsilon_{\text{m}}\right]}}\times \times\left(\frac{\omega_p}{c}\right)^3\left(\frac{\omega_p}{\omega}\right)^2\frac{v_{\text{F}}}{2R}\mathcal{F}_{\perp(\parallel)}(\varrho_{\text{eff}}), \tag{29}$$

where depolarization factors and size-dependent functions are determined as follows[31,46]:

– for cylinder, which is equivalent to prolate spheroid

$$\mathcal{L}_\parallel = \frac{\varrho_{\text{eff}}^2}{2\left(1-\varrho_{\text{eff}}^2\right)^{3/2}}\left(\ln\frac{1+\sqrt{1-\varrho_{\text{eff}}^2}}{1-\sqrt{1-\varrho_{\text{eff}}^2}}-2\sqrt{1-\varrho_{\text{eff}}^2}\right), \qquad \mathcal{L}_\perp = \frac{1}{2}\left(1-\mathcal{L}_\parallel\right); \tag{30}$$

$$\mathcal{F}_\perp(\varrho_{\text{eff}}) = \left(1-\varrho_{\text{eff}}^2\right)^{-\frac{3}{2}}\times \times\left\{2\left(\frac{3}{4}-\varrho_{\text{eff}}^2\right)\left(\frac{\pi}{2}-\arcsin\varrho_{\text{eff}}\right)+\varrho_{\text{eff}}\left(\frac{3}{2}-\varrho_{\text{eff}}^2\right)\sqrt{1-\varrho_{\text{eff}}^2}\right\} \tag{31}$$

$$\mathcal{F}_\parallel(\varrho_{\text{eff}}) = \left(1-\varrho_{\text{eff}}^2\right)^{-\frac{3}{2}}\times \times\left\{\frac{\pi}{2}-\arcsin\varrho_{\text{eff}}+\varrho_{\text{eff}}\left(1-2\varrho_{\text{eff}}^2\right)\sqrt{1-\varrho_{\text{eff}}^2}\right\}; \tag{32}$$

– for disc, which is equivalent to oblate spheroid

$$\mathcal{L}_\parallel = \frac{\varrho_{\text{eff}}^2}{2\left(\varrho_{\text{eff}}^2-1\right)^{3/2}}\left(\sqrt{\varrho_{\text{eff}}^2-1}-\text{arctg}\sqrt{\varrho_{\text{eff}}^2-1}\right), \qquad \mathcal{L}_\perp = \frac{1}{2}\left(1-\mathcal{L}_\parallel\right); \tag{33}$$

$$\mathcal{F}_\perp(\varrho_{\text{eff}}) = \frac{1}{2}\left(\varrho_{\text{eff}}^2-1\right)^{-\frac{3}{2}}\times \times\left\{\varrho_{\text{eff}}\left(2\varrho_{\text{eff}}^2-3\right)\sqrt{\varrho_{\text{eff}}^2-1}+\left(4\varrho_{\text{eff}}^2-3\right)\ln\left(\varrho_{\text{eff}}+\sqrt{\varrho_{\text{eff}}^2-1}\right)\right\}; \tag{34}$$

$$\mathcal{F}_\parallel(\varrho_{\text{eff}}) = \left(\varrho_{\text{eff}}^2-1\right)^{-\frac{3}{2}}\times \times\left\{\varrho_{\text{eff}}\left(2\varrho_{\text{eff}}^2-1\right)\sqrt{\varrho_{\text{eff}}^2-1}-\ln\left(\varrho_{\text{eff}}+\sqrt{\varrho_{\text{eff}}^2-1}\right)\right\}. \tag{35}$$

Let us point out that the relation between aspect ratio and effective aspect ratio for cylinders and discs [31,46]

$$\varrho_{\text{eff}} = \frac{\sqrt{3}}{2}\varrho, \tag{36}$$

and the aspect ratios for cylinders and discs

$$\varrho = \frac{2R}{l}, \quad \varrho = \frac{D}{H}. \tag{37}$$

Thereafter the relations (2), (3), (10), (11), (17), (18) taking into account formulae (12), (14) – (16), (19), (24) – (37) are going to be used in order to obtain the numerical results.

3. RESULTS OF THE CALCULATIONS AND THEIR DISCUSSION

The frequency dependence of polarizability, absorption and scattering cross-sections, overheating and radiation efficiency and Joule number size dependence were calculated for spherical, cylindrical and disc nanoparticles of different metals in Teflon ($\epsilon_{\text{m}} = 2.3$, $\kappa = 0{,}25\ \frac{\text{W}}{\text{m}\cdot\text{K}}$). The parameters of metals, required for the calculations, are given in Table 1.

Table 1 – The parameters of metals (a_0 is the Bohr radius) (see, for example, [33, 46] and references therein)

Metals	Value				
	r_s / a_0	m^* / m_e	ϵ^∞	$\hbar\omega_p$, eV	$\hbar\gamma_{\text{bulk}}$, eV
Cu	2.11	1.49	12.03	12.6	0.024
Au	3.01	0.99	9.84	9.07	0.023
Ag	3.02	0.96	3.7	9.17	0.016
Pt	3.27	0.54	4.42	15.2	0.069
Pd	4.00	0.37	2.52	9.7	0.091

The frequency dependencies for the real and imaginary parts, as well as polarizability module of spherical nanoparticle and the diagonal components of the polarizability tensor of cylindrical and disc particles are given if Fig. 3. The common feature of the corresponding curves is the fact that the function $\mathrm{Re}\,\alpha(\omega)$ is alternating function for all shapes of nanoparticles, and $\mathrm{Im}\,\alpha(\omega) > 0$ in the frequency range, which is under the study. Moreover, $\mathrm{Re}\,\alpha \sim \mathrm{Im}\,\alpha$ for all shapes of particles, which are under the study, hence, the curves $|\alpha(\omega)|$ have the features of both the curves $\mathrm{Re}\,\alpha(\omega)$ and curves $\mathrm{Im}\,\alpha(\omega)$. Let us point out the differences of the curves $\mathrm{Im}\,\alpha(\omega)$:

1) amplitude of $\max\{\mathrm{Im}\,\alpha\}$ for sphere is significantly less than amplitude of $\max\{\mathrm{Im}\,\alpha_{\perp(\parallel)}\}$ for cylinder and disc;

2) $\max\{\mathrm{Im}\,\alpha_\parallel\} > \max\{\mathrm{Im}\,\alpha_\perp\}$ for cylinder, while for disc on the contrary $\max\{\mathrm{Im}\,\alpha_\parallel\} < \max\{\mathrm{Im}\,\alpha_\perp\}$;

3) $\Delta\omega_{sp}^{\text{disk}} \ll \Delta\omega_{sp}^{\text{cyl}}$ for the frequencies of the transverse and longitudinal SPR, which correspond to $\max\{\mathrm{Im}\,\alpha_{\perp(\parallel)}\}$. At the same time, $\omega_{sp}^{\perp} > \omega_{sp}^{\parallel}$ for cylinders, and, on the contrary, $\omega_{sp}^{\perp} < \omega_{sp}^{\parallel}$ for discs, that is the frequency of SPR, which corresponds to the greater size of cylinder / disc, is the least.

The frequency dependencies for the absorption cross-section and scattering cross-section for the particles of all shapes, which are under the study, are given in Fig. 4. Let us point out that the number and location of $\max\{C_{\text{abs}}\}$ and $\max\{C_{\text{sca}}\}$ fully complies with the case $\mathrm{Im}\,\alpha(\omega)$. Thus, in the case of spherical nanoparticles, one maximum is observed, while for cylindrical and disc nanoparticles, two maximums are observed each. In the case of disc nanoparticles, these maxima practically merge, whereas for cylindrical particles the distance between them is rather large (~ 2 eV). The proximity of $\max\{C_{\text{abs}}\}$ for discs is explained by the fact that for them the splitting of the frequencies of SPR $\Delta\omega_{sp} \cong \gamma_{\text{bulk}}$ [47]. It should also be pointed out that the proximity, and in some cases the merging of the maximums of absorption and scattering cross-sections is also characteristic of nanoparticles of other shapes, equivalent to which is oblate spheroid, for example, bicones / bipyramids, where $h < 2r$ ($h < 2r_{\text{red}}$), where h – height, r (r_{red}) – radius (reduced radius) of the base of bicone (bipyramid) [46].

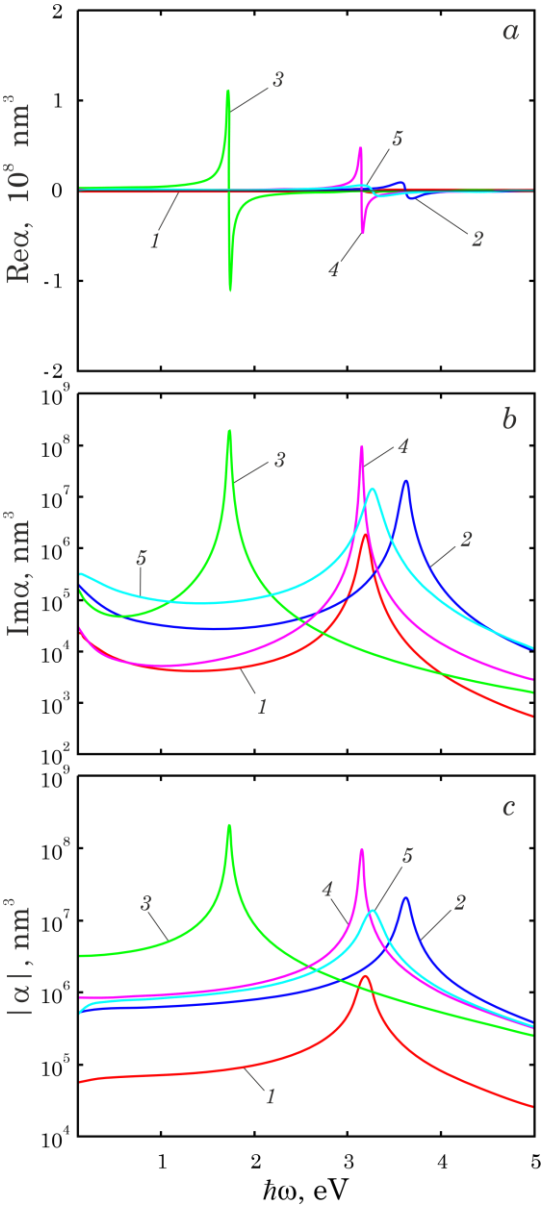

Fig. 3 – The frequency dependencies for the real (*a*) and imaginary (*b*) parts, as well as module (*c*) of the polarizability of silver nanoparticles of the different geometrical form in Teflon: *1* – α spherical particle with $R = 40$ nm; *2* and *3* – $\alpha_\perp$ and $\alpha_\parallel$ cylindrical particle ($2r = 47.7$ nm, $l = 150$ nm); *4* and *5* – $\alpha_\perp$ and $\alpha_\parallel$ disc particle ($D = 116.8$ nm, $H = 25$ nm)

The frequency dependences for the overheating of spherical, cylindrical and disc silver nanoparticles are shown in Fig. 5. Let us point out that in the second biological transparency window (band II) the overheating of the particles of all shapes is ~ 1 K, while in the first biological transparency window (band I) $\Delta T_{\max} \sim 10^3$ K for cylindrical particle. At the same time, for spherical and disc nanoparticles, the overheating increases only slightly compared to the second biological transparency window.

This is due to the fact that $\Delta T \sim C_{\text{abs}}$, and, hence, $\Delta T_{\max}$ correspond to the surface plasmonic resonances. It is a known fact that for disc and spherical particles the frequency of SPR significantly exceeds the upper boundary of the first biological window of transparency, while for cylindrical nanoparticles the frequency of the longitudinal SPR is significantly (two times) less than the frequency of transverse SPR and falls, depending on the aspect ratio, either into the red or near-infrared frequency range (the first biological window of transparency).

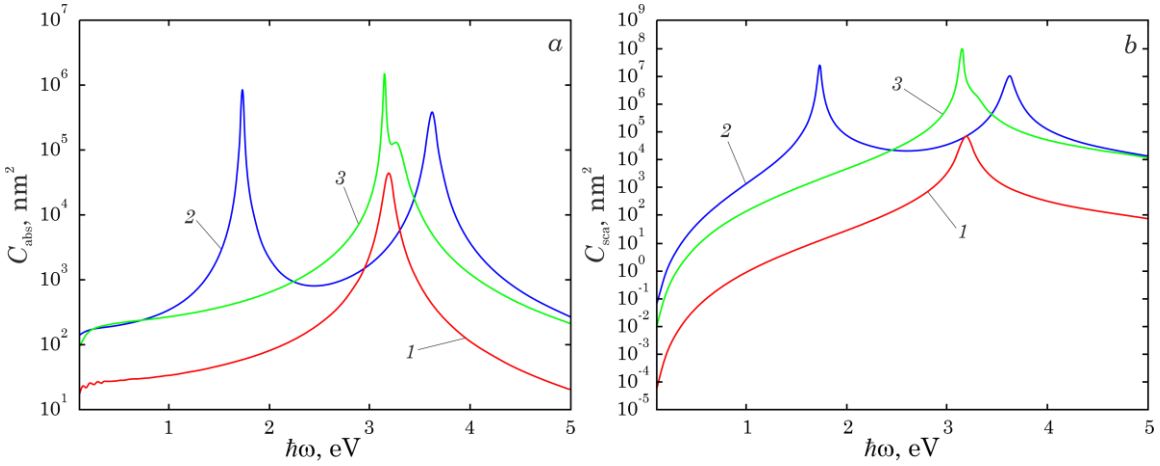

Fig. 4 – The frequency dependencies for the absorption cross-section (*a*) and scattering cross-section (*b*) of metallic nanoparticles Ag of the different shape in Teflon: *1* – spherical; *2* – cylindrical; *3* – disc-shaped under the same values of the geometric parameters as in Fig. 3

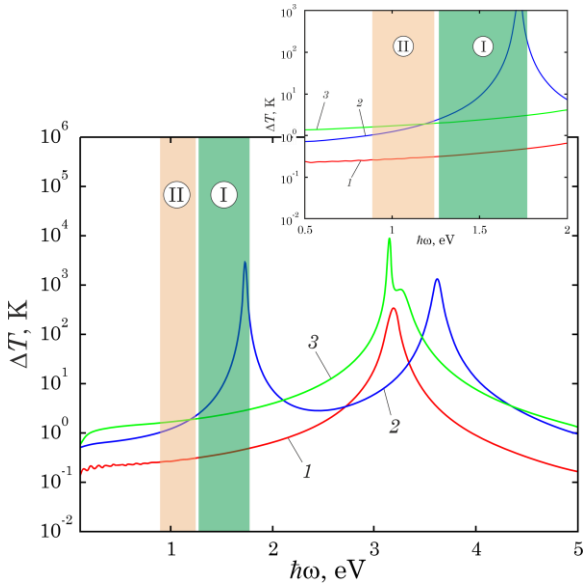

Fig. 5 – The frequency dependencies for the overheating of nanoparticles Ag of the shapes, which are under the study, in Teflon (the spectral interval $0.5 \div 2.0$ eV is highlighted in the inset). The values of the geometric parameters are the same as in Fig. 3

The dependencies $\Delta T(\omega)$ for the nanoparticles of the shapes, which are under the study, of the different sizes and produced of different metals are demonstrated in Fig. 6 – 8. In the case of spherical silver nanoparticles, the position $\Delta T_{\max}$ is independent of the particle radius, while its amplitude and overheating in the biological transparency window increase with increasing radius (Fig. 6, *a*). For spherical particles of different metals with $R = 40$ nm the maxima of the overheating are located in the order $\text{Au} \to \text{Cu} \to \text{Ag} \to \text{Pd} \to \text{Pt}$ in which the plasma frequency ω_p of these metals increases. In the same order, the magnitude of the overheating in biological transparency windows also increases, remaining in magnitude ~ 1 K.

In the case of silver cylindrical particles, the positions of the overheating maxima depend significantly on the radius and length of the cylinder and, consequently, on the aspect ratio (Fig. 7, *a*). Thus, with increasing aspect ratio ($\varrho \to 1$) the splitting of the overheating maxima decreases (the maximus are "attracted"). It should also be pointed out that with increasing aspect ratio the maximum of the overheating shifts from the second biological window of transparency (the case of small aspect ratios) first to the first window, and then leaves the specified frequency intervals altogether, and the overheating for such cases will be several degrees. Such behaviour of the first maximum ΔT is due to the fact that the longitudi-

nal SPR frequency for the nanocylinder increases with increasing aspect ratio, as shown in [30]. In the case of cylindrical nanoparticles of different metals with the fixed aspect ratio, we point out that for most plasmonic metals the first maximum of the overheating falls into the second biological window of transparency, except for platinum, for which the plasmonic frequency is the highest.

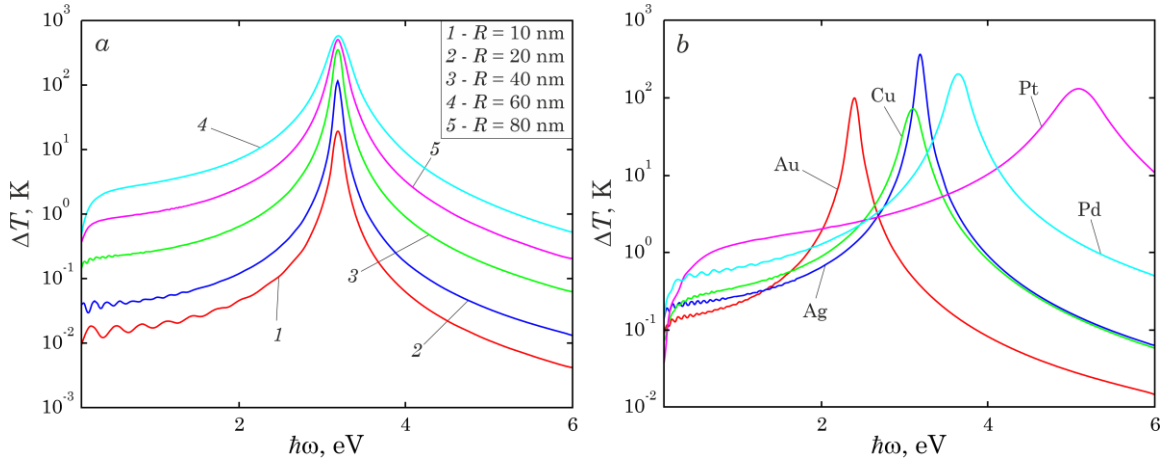

Fig. 6 – The frequency dependencies for the overheating of spherical nanoparticles Ag with the different radius (*a*) and nanoparticles of different metals with the radius $R = 40$ nm (*b*) in Teflon

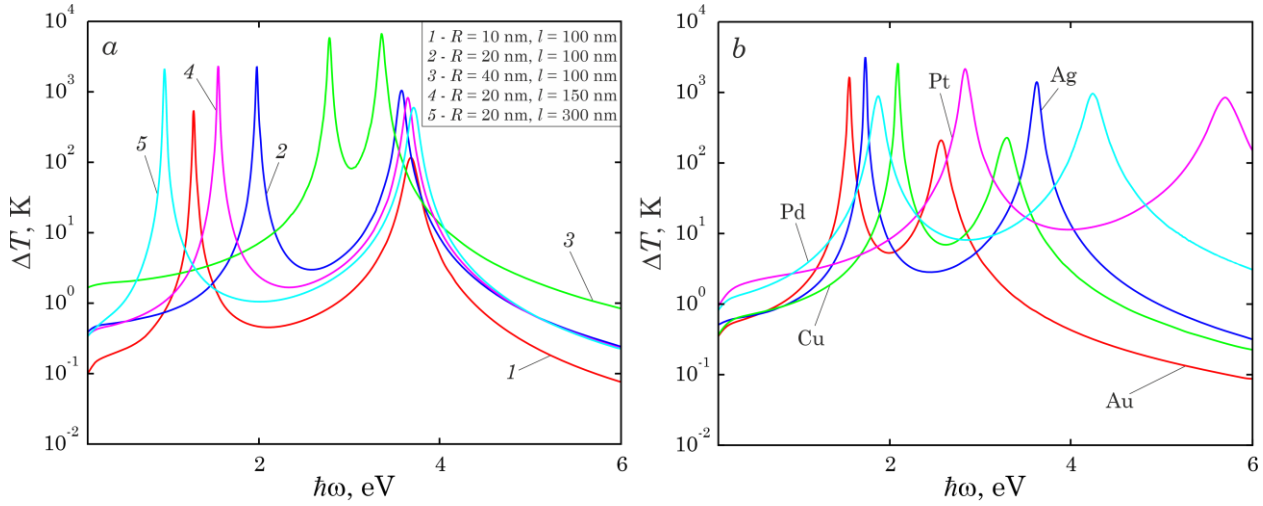

Fig. 7 – The frequency dependencies for the overheating of cylindrical nanoparticles Ag of the different sizes (*a*) and the nanoparticles of different metals with the parameters $2r = 47.7$ nm, $l = 150$ nm (*b*) in Teflon

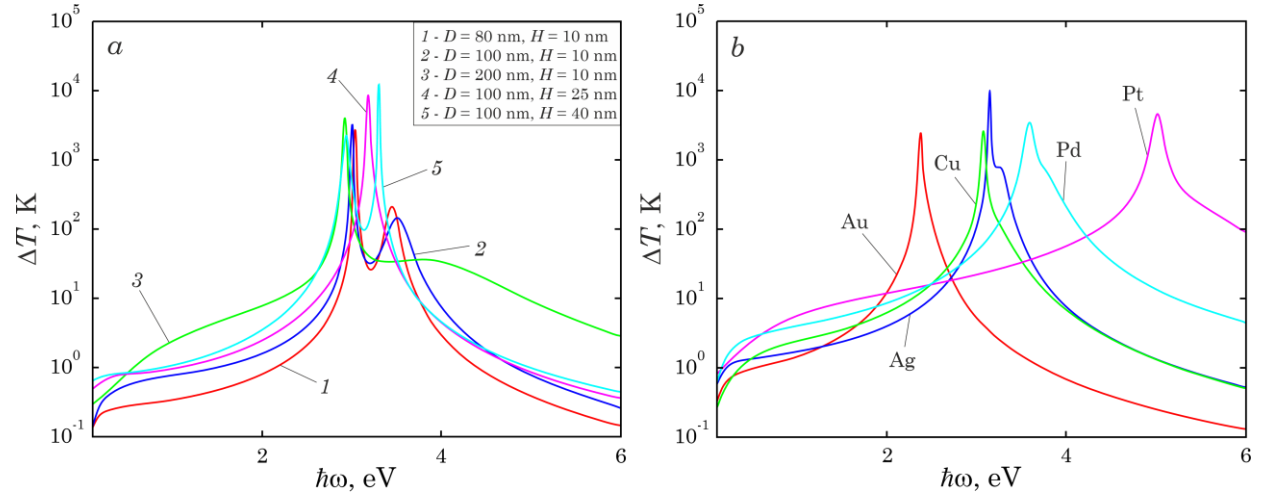

Fig. 8 – The frequency dependencies for the overheating of disc nanoparticles Ag of the different sizes (*a*) and nanoparticles of different metals with the parameters $D = 116.8$ nm, $H = 25$ nm (*b*) in Teflon

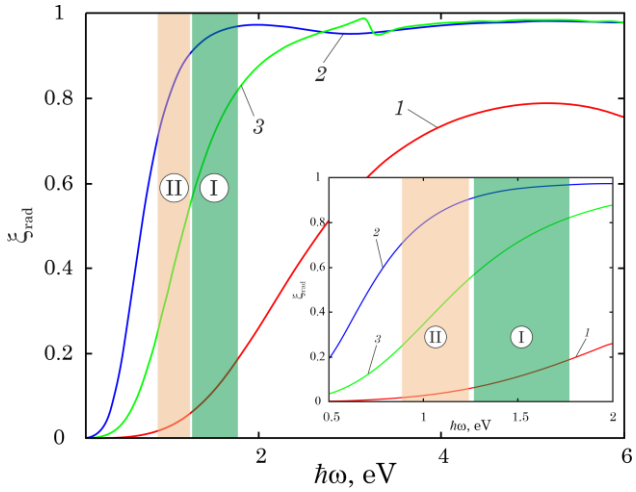

Fig. 9 – The frequency dependencies for the radiation efficiency of the nanoparticles Ag of the shapes, which are under the study, in Teflon (the spectral interval $0.5 \div 2.0$ eV is highlighted in the inset). The values of the geometric parameters are the same as in Fig. 3

For disc particles, the only thing in common with the previous case is the presence of two overheating maxima and their shifts under the variation of the disc diameter and height (aspect ratio). In contrast to cylindrical nanoparticles, the distance between the overheating maxima is significantly smaller, the first overheating maximum corresponds to the transverse SPR frequency and the second to the longitudinal SPR frequency. Moreover, all overheating maxima are outside the biological transparency windows, in which the overheating ranges from fractions of a degree to a few degrees, and the distance between maxima (maxima splitting) increases with increasing aspect ratio (Fig. 8, *a*). This fact correlates with the fact established in [47] that the splitting of SPR increases with increasing aspect ratio. It should also be pointed out that the number and position of the overheating maxima depend on the material of the disc nanoparticles (Fig. 8, *b*). For the same diameters and heights of nanodiscs, the second maximum of the overheating is clearly distinguishable only for the discs Ag.

The curves of the frequency dependencies of the radiation efficiency for particles of all studied shapes with the same volume (the frequency interval with biological transparency windows is highlighted in the inset) are given in Fig 9. In the whole investigated frequency range (including frequencies, which correspond to biological transparency windows) the radiation efficiency increases in the series of nanoparticle shapes "sphere → disc → cylinder". Taking into account this and the fact that the first maximum of the overheating of cylindrical particles with the relatively small aspect ratio falls within one of the biological transparency windows, in cases when negligible heating is required, spherical and disc-shaped nanoparticles or cylindrical nanoparticles with $\varrho \to 1$ are useful.

The size dependences of the Joule number for spherical, cylindrical, and disk-shaped nanoparticles are shown in Fig. 10. The results of the calculations indicate that the ability to generate heat is minimal for disk particles. In turn, for cylindrical particles, the Joule number under the small values of the aspect ratio reaches the maximum ($J_0 \sim 10^3$) for light whose

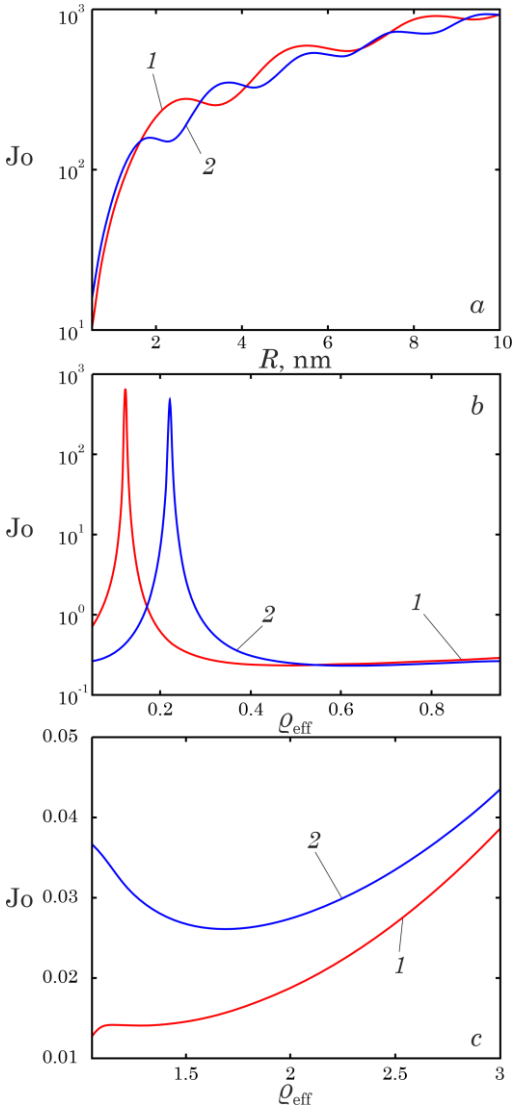

Fig. 10 – The size dependencies of the Joule number for spherical (*a*), cylindrical (*b*) and disc (*c*) silver nanoparticles in Teflon under: *1* – $\hbar\omega = 1.0$ eV , *2* – $\hbar\omega = 1.5$ eV .

frequencies fall within the first and second biological transparency windows. In the case of spherical nanoparticles, the Joule number increases with increasing radius, while for cylinders and disks $J_0 < 1$ under the increase in the aspect ratio.

4. CONCLUSIONS

The relations for the frequency dependence of the overheating of metallic spherical, cylindrical, and disk nanoparticles have been obtained, and the size dependences of the effective relaxation rate for cylindrical and disk particles have been found using the equivalent spheroid approach.

It has been shown that for nanodiscs the splitting of SPR frequencies is much less than for nanocylinders, and the smaller of the SPR frequencies corresponds to the greater size of 1*D*-particle. Thus, for cylinder the smaller is the longitudinal SPR frequency, and for disk – the transverse SPR frequency.

It has been established that the number and location of the maximums of the absorption and scattering cross-sections correspond to the cases of the frequency dependences of the imaginary part and polarizability modulus of nanoparticles of the shapes, which are under the study. Therefore, the absorption and scattering cross-sections for spherical nanoparticles have one maximum, while they have two maxima for cylindrical and disk particles, and for disk particles they are either closely located or practically indistinguishable.

It has been demonstrated that the number and spectral positions of the overheating maxima also depend on the shape of the nanoparticles as they correspond to the surface plasmonic resonance frequencies. Thus, the frequency dependences of the overheating of spherical and disk particles have one maximum or two closely located maxima lying outside the biological windows of transparency, while cylindrical particles have two sufficiently distant maxima, the first of which may fall within the biological windows of transparency.

It has been proved that the position of the overheating maximum of spherical nanoparticle does not depend on its radius, while the position of the overheating maxima of 1*D*-particles depends on the value of the aspect ratio. Thus, in the case of cylindrical particles, there is an "attraction" of maxima as the aspect ratio increases, and in the case of disk particles, there is a "repulsion" of overheating maxima as the aspect ratio increases.

It has been shown that the "blue" shift of the overheating maxima for particles of all forms in the series of metals $\mathrm{Au} \to \mathrm{Ag} \to \mathrm{Cu} \to \mathrm{Pd} \to \mathrm{Pt}$ is determined by the increase of the plasma frequency in just such a sequence.

The results of the calculations of the frequency dependences of radiation efficiency of silver nanoparticles of all shapes with the same volume show that in the whole frequency range, which is under study, the radiation efficiency increases in the series of shapes "sphere – disk – cylinder".

The principal difference (both qualitative and quantitative) in the size dependences of the Joule number for particles of the studied forms has been demonstrated. Thus, the ability to generate heat at frequencies from the first and second biological transparency windows was found to be lowest for disk particles, while for cylindrical particles the Joule number reaches the maximum at small aspect ratios, and for spherical particles increases with increasing radii.

REFERENCES

1. G. Baffou, P. Berto, E. Bermúdez Ureña, R. Quidant, S. Monneret, J. Polleux, H. Rigneault, *ACS Nano.* **7**, 6478 (2013).
2. L. Sixdenier, G. Baffou, C. Tribet, E. Marie, *J. Phys. Chem. Lett.* **14**, 11200 (2023).
3. Z.J. Coppens, W. Li, D.G. Walker, J.G. Valentine, *Nano Lett.* **13**, 1023 (2013).
4. J.M. Luther, P.K. Jain, T. Ewers, A.P. Alivisatos, *Nat. Mater.* **10**, 361 (2011).
5. P. Han, W. Martens, E.R. Waclawik, S. Sarina, H. Zhu, *Part. Part. Syst. Charact.* **35**, 1700489 (2018).
6. L. Jauffred, A. Samadi, H. Klingberg, P.M. Bendix, L.B. Oddershede, *Chem. Rev.* **119**, 8087 (2019).
7. M. Alrahili, V. Savchuk, K. McNear, A. Pinchuk, *Sci. Rep.* **10**, 18790 (2020).
8. A.V. Korotun, N.I. Pavlyshche, *Phys. Metals Metallogr.* **122**, 941 (2021).
9. G. Baffou, R. Quidant, *Laser Photon. Rev.* **7**, 171 (2013).
10. H. Duan, R. Chen, Y. Zheng, C. Xu, *Opt. Express* **26**, 29956 (2018).
11. S. Farooq, C.V. Vital, L.A. Gómez-Malagón, R.E. de Araujo, D. Rativa, *Sol. Energy* **208**, 1181 (2020).
12. A.M. Vieira, N.T.C. Oliveira, K.T.P.B. Silva, A.S. Reyna, *J. Phys. Chem. C* **125**, 19653 (2021).
13. C.V. Vital, S. Farooq, R.E. de Araujo, D. Rativa, L.A. Gómez-Malagón, *Appl. Therm. Eng.* **190**, 116799 (2021).
14. M.D. Sherar, J. Trachtenberg, S.R.H. Davidson, M.R. Gertner, *Int. J. Hyperth.* **20**, 757 (2004).
15. P.R. Stauffer, *Med. Phys.* **40**, 067302 (2013).
16. J. Chen, C. Glaus, R. Laforest, Q. Zhang, M. Yang, M. Gidding, M.J. Welch, Y. Xia, *Small* **6**, 811 (2010).
17. A. Bucharskaya, G. Maslyakova, G. Terentyuk, A. Yakunin, Y. Avetisyan, O. Bibikova, E. Tuchina, B. Khlebtsov, N. Khlebtsov, V. Tuchin, *Int. J. Mol. Sci.* **17**, 1295 (2016).
18. Y. Liu, B.M. Crawford, T. Vo-Dinh, *Immunotherapy* **10**, 1175 (2018).
19. J. Li, F. Zhao, Y. Deng, D. Liu, C.H. Chen, W.C. Shih, *Opt. Express* **26**, 16893 (2018).
20. K. Metwally, S. Mensah, G. Baffou, *J. Phys. Chem. C* **119**, 28586 (2015).
21. B.S.L. Lalonde, É. Boulais, J.J. Lebrun, M. Meunier, *Biomed. Opt. Express* **4**, 490 (2013).
22. S. Patskovsky, M. Qi, M. Meunier, *Analyst* **145**, 523 (2020).
23. T.E. Pylaev, Y. Efremov, E.S. Avdeeva, A.A. Antoshin, A.I. Shpichka, T.M. Khlebnikova, P. Timashev, N.G. Khlebtsov, *ACS Appl. Nano Mater.* **4**, 13206 (2021).
24. J.B. Khurgin, G. Sun, W.T. Chen, W.Y. Tsai, D.P. Tsai, *Sci. Rep.* **5**, 17899 (2015).
25. A.M. Smith, M.C. Mancini, S. Nie, *Nat. Nanotechnol.* **4**, 710 (2009).
26. E.B. Dickerson, E.C. Dreaden, X. Huang, I.H. El-Sayed, H. Chu, S. Pushpanketh, J.F. McDonald, M.A. El-Sayed, *Cancer Lett.* **269**, 57 (2008).
27. A.M. Gobin, M.H. Lee, N.J. Halas, W.D. James, R.A. Drezek, J.L. West, *Nano Lett.* **7**, 1929 (2007).
28. A.V. Korotun, A.A. Koval', I.N. Titov, *J. Appl. Spectrosc.* **87**, 240 (2020).
29. J. Chen, D. Wang, J. Xi, L. Au, A. Siekkinen, A. Warsen, Z.Y. Li, H. Zhang, Y. Xia, X. Li, *Nano Lett.* **7**, 1318 (2007).
30. A.V. Korotun, Ya.V. Karandas, V.I. Reva, *Ukr. J. Phys.* **67**,

849 (2022).
31. M.H. Niemz, *Laser Safety. In Biological and Medical Physics, Biomedical Engineering*, 249 (Springer: Berlin/Heidelberg, Germany: 2007)
32. A.V. Korotun, V.V. Pogosov, *Phys. Solid State* **63**, 122 (2021).
33. A.V. Korotun, A.O. Koval, V.V. Pogosov, *Ukr. J. Phys.* **66**, 518 (2021).
34. A.V. Korotun, N.A. Smirnova, V.I. Reva, I.M. Titov, G.M. Shilo, *Condens. Matter Phys.* **26**, 43704 (2023).
35. A. Korotun, *XII International Scientific Conference "Functional Basis of Nanoelectronics" (FBN-2021)*, 112 (Kharkiv – Odesa: Collection of Scientific Works: 2021).
36. N.A. Smirnova, R.O. Malysh, A.V. Korotun, V.I. Reva, I.M. Titov, *J. Nano- Electron. Phys.* **13**, 05010 (2021).
37. G. Baffou, H. Rigneault, *Phys. Rev. B* **84**, 035415 (2011).
38. C.F. Bohren, D.R. Huffman, *Absorption and Scattering of Light by Small Particles*, (John andWiley and Sons: Hoboken, NJ, USA, 2008).
39. D. Jaque, L.M. Maestro, B. del Rosal, P. Haro-Gonzalez, A. Benayas, J.L. Plaza, E.M. Rodríguez, J.G. Solé, *Nanoscale* **6**, 9494 (2014).
40. N.S. Abadeer, C.J. Murphy, *J. Phys. Chem. C* **120**, 4691 (2016).
41. A. Lalisse, G. Tessier, J. Plain, G. Baffou, *J. Phys. Chem. C* **119**, 25518 (2015).
42. A.N. Yakunin, Y.A. Avetisyan, V.V. Tuchin, *J. Biomed. Opt.* **20**, 051030 (2015).
43. J. Morales-Dalmau, C. Vilches, I. de Miguel, V. Sanz, R. Quidant, *Nanoscale* **10**, 2632 (2018).
44. N. Khlebtsov, L.A. Dykman, *J. Quant. Spectrosc. Radiat. Transf.* **111**, 1 (2010).
45. A.V. Korotun, N.I. Pavlyshche, *Functional Mater.* **29**, 567 (2022).
46. A.V. Korotun, *Ukr. J. Phys.* **68** No 10, 695 (2023).
47. A.V. Korotun, N.I. Pavlishche, *Opt. Spectrosc.* **130**, 269 (2022).

Вплив геометрії на термоплазмонні явища у металевих наночастинках

В.І. Рева[1], Р.Ю. Корольков[1], М.А. Швидкий[1], А.В. Коротун[1,2], Є.В. Стеганцев[3], О.С. Гнатенко[1,4]

[1] *Національний університет «Запорізька політехніка», 69063 Запоріжжя, Україна*
[2] *Інститут металофізики ім. Г. В. Курдюмова НАН України, 03142 Київ, Україна*
[3] *Запорізький національний університет, 69600 Запоріжжя, Україна*
[4] *Харківський національний університет радіоелектроніки, 61166 Харків, Україна*

У роботі досліджуються термоплазмонні явища у металевих наночастинках різної геометрії. Отримано співвідношення для частотних залежностей перегріву наночастинок та радіаційної ефективності, а також розмірної залежності числа Джоуля, що характеризує здатність наночастинок генерувати тепло. При цьому розмірні залежності ефективної швидкості релаксації електронів для циліндричних та дискових частинок визначені в рамках підходу еквівалентного сфероїду. Частотні залежності поляризовності, перерізів поглинання та розсіювання, перегріву, радіаційної ефективності та розмірні залежності числа Джоуля розраховувалися для сферичних, циліндричних і дискових наночастинок різних розмірів та різних металів. Показано, що кількість та положення максимумів перерізів поглинання та розсіювання та перегріву металевих наночастинок залежить від їхньої геометрії, а у випадку 1*D*-частинок і від їх розмірів (аспектного відношення). При цьому розщеплення цих максимумів для циліндричних частинок значно більше, ніж для дискових. Розрахунки демонструють, що перегрів наночастинок у біологічних вікнах прозорості складає від часток до декількох градусів, крім випадку наноциліндрів із малим аспектним відношенням, коли максимуми перегріву срібних наночастинок потрапляють у перше біологічне вікно прозорості. Встановлено, що матеріал наночастинок також суттєво впливає на положення максимуму їхнього перегріву та визначається величиною плазмової частоти. Продемонстровано доцільність застосування сферичних, дискових і коротких циліндричних наночастинок у застосуваннях, де необхідний незначний перегрів у біологічних вікнах прозорості. У випадку ж, коли необхідний значний перегрів доцільним є використання довгих наноциліндрів. Виявлено принципові відмінності в поведінці числа Джоуля (здатності генерувати тепло) для частинок різної геометрії при зміні їхнього радіусу / аспектного відношення.

Ключові слова: Поляризовність, Переріз поглинання та розсіювання, Перегрів, Радіаційна ефективність, Число Джоуля, Ефективна швидкість релаксації.